

Transmission Line Characterization of Undercut-Ridge Traveling-Wave Electroabsorption Modulators

Matthew M. Dummer, Jonathan Klamkin, Erik J. Norberg, Anna Tauke-Pedretti, James W. Raring, and Larry A. Coldren

Abstract—An experimental analysis of the electrical properties of traveling-wave electroabsorption modulators with undercut waveguides is presented. Modulators of varying ridge widths and amounts of undercut are fabricated and tested to compare characteristic impedance, effective index, microwave loss, and optical bandwidth. We demonstrate effective velocity matching and >40 -GHz 3-dB bandwidth for a $400\text{-}\mu\text{m}$ -long device.

Index Terms—Electroabsorption, traveling-wave devices, undercut etching.

I. INTRODUCTION

ELECTROABSORPTION modulators (EAMs) have proven to be important devices for modulation of optical signals due to their compact size, high speed, low drive voltage, and ease of integration with semiconductor lasers. For traveling-wave modulators (TW-EAMs), transmission line electrodes are utilized such that the electrical drive signal interacts coherently with the propagating light thereby surpassing the traditional resistance–capacitance (RC) bandwidth limitation. However, the modulator capacitance still plays an important role in the frequency response. Traveling-wave devices are limited by impedance mismatch, velocity mismatch, and microwave loss, all of which are affected by the capacitance per length of the EAM. Recently, improved bandwidth of TW-EAMs has been demonstrated by undercutting of the waveguide core with selective wet etching [1], [2]. This technique allows for significant reduction of the diode junction capacitance while still maintaining a wide cladding for low series resistance [3]. Undercut etching has also been shown to lower the optical scattering loss by reducing the overlap between the mode and the outer sidewalls of the cladding layers [1].

In this work, we have developed a fabrication process for integrating undercut waveguide TW-EAMs with sampled grating DBR lasers for high-speed tunable transmitters [4]. As an optimization study, we have fabricated several discrete TW-EAMs with varied core and cladding dimensions in order to characterize their transmission line properties. Here, we present the

Manuscript received February 16, 2008; revised March 28, 2008. This work was supported by Defense Advanced Research Projects Agency (DARPA) MTO-LASOR Grant W911NF-04-9-0001.

The authors are with the Department of Electrical and Computer Engineering and the Department of Materials, University of California Santa Barbara, Santa Barbara, CA 93106 USA (e-mail: dummer@engineering.ucsb.edu).

Color versions of one or more of the figures in this letter are available online at <http://ieeexplore.ieee.org>.

Digital Object Identifier 10.1109/LPT.2008.926908

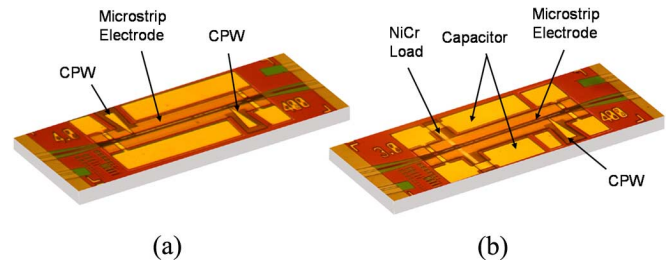


Fig. 1. Fabricated TW-EAMs with (a) two-port CPW pad design and (b) integrated termination.

experimental results of this study which demonstrate the dependence of the characteristic impedance, electrical effective index, and microwave loss on the modulator geometry over a wide design space. This study demonstrates improved velocity matching, increased impedance, and reduced loss for undercut waveguides with core dimensions as narrow as $1.4\ \mu\text{m}$.

II. DESIGN AND FABRICATION

We have designed modulators with two different electrode configurations for these characterization experiments. As shown in Fig. 1, the first was designed with both input and output coplanar waveguide pads for two-port electrical characterization. The second was designed with an integrated matched termination to reduce electrical reflections [5]. The modulator microstrip electrodes were $400\ \mu\text{m}$ long, $6\ \mu\text{m}$ wide, and the width of the underlying ridges were varied on the mask from 2.5 to $5.0\ \mu\text{m}$. Laterally flared, curved waveguides were used at both facets to reduce optical reflections. The epitaxial layer structure for these modulators consisted of a 350-nm InGaAsP core surrounded by $1.8\ \mu\text{m}$ each of InP for the upper and lower n- and p-doped cladding. The core contained a stack of ten quantum wells with a band edge corresponding to photoluminescence emission wavelength of $1465\ \text{nm}$. A sulfur-doped substrate was used to allow for backside n-contacts while $150\ \text{nm}$ of highly doped p-InGaAs above the upper cladding provided an ohmic contact layer on the p-side. The optical waveguides for this device consisted of surface ridges at the facets which were tapered to deeply etched ridges for the modulation region of the TW-EAM. The ridges were patterned and defined using a combination of wet and dry etching before performing a selective wet etch to reduce the width of the InGaAsP core. Three pieces of the same wafer were processed, one with no undercut etching, and the other two with undercut etch times of 22 and 40 min in $\text{H}_2\text{SO}_4 : \text{H}_2\text{O}_2 : \text{H}_2\text{O}$ solution (1 : 1 : 10). The total reduction in the active width of the two samples was measured to be 0.9

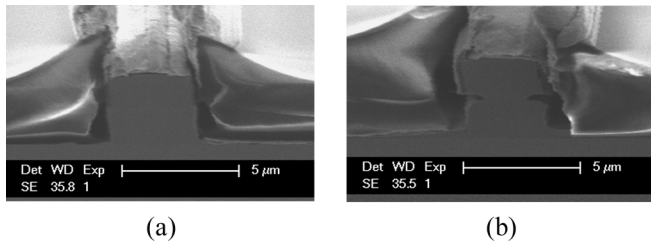


Fig. 2. Scanning electron microscope cross section of (a) deep-etched and (b) undercut-ridge waveguide structures designed for a ridge width of $3.0\ \mu\text{m}$.

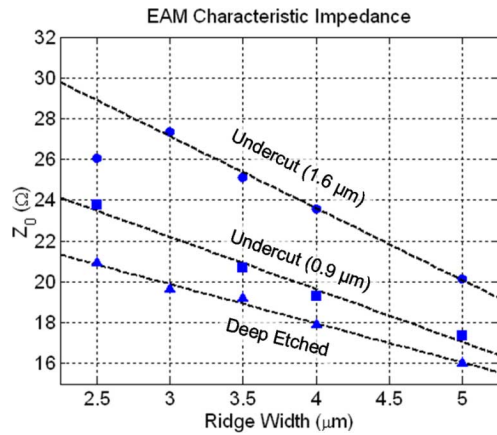


Fig. 3. Measured characteristic impedance versus ridge width for varied amount of undercut.

and $1.6\ \mu\text{m}$, respectively. The waveguides were then buried with photodefined benzocyclobutene (BCB) as a low- k dielectric. A via was etched through the BCB to expose the ridge-top before the final metallizations to form the p-side contact and thin-film NiCr resistor. An electron micrograph of the cross sections of the deeply etched (no undercut) and 40-min undercut-etched devices are shown in Fig. 2.

III. CHARACTERIZATION EXPERIMENTS

The TW-EAM transmission line structures were measured and analyzed using a two-port scattering parameter method [6]. For these experiments, all of the modulators tested were the two-terminal implementation shown in Fig. 1(a). The devices were directly probed with $50\text{-}\Omega$ ground-signal-ground coplanar probes on both sides of the EAM and measurements were taken with an HP 3910C network analyzer. The measurement setup was calibrated to the ends of the probes using a calibration substrate, to accurately isolate the response of the device under test. All four electrical S-parameters were measured over a range of DC reverse biases; however, no change in response was observed beyond $-2\ \text{V}$. For simplicity, no optical input power was present during the measurements. The characteristic impedance, effective index, and microwave loss were then extracted from the S-parameters using the ABCD matrix method [6].

All devices tested exhibited well behaved transmission line characteristics over the range of 130 MHz to 20 GHz. Fig. 3 shows the variation in characteristic impedance (Z_0) of 14 TW-EAMs with different ridge widths and levels of undercut. Only the impedance measured at 20 GHz (-3-V bias) is shown since there was little variation over the frequency range. The measured values range from 15 to $27\ \Omega$ with smaller diode areas

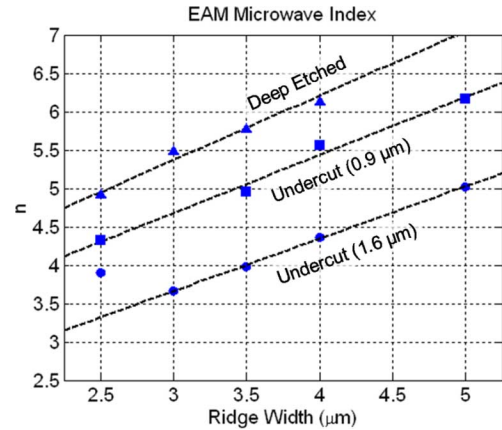


Fig. 4. Measured electrical effective index versus ridge width and undercut.

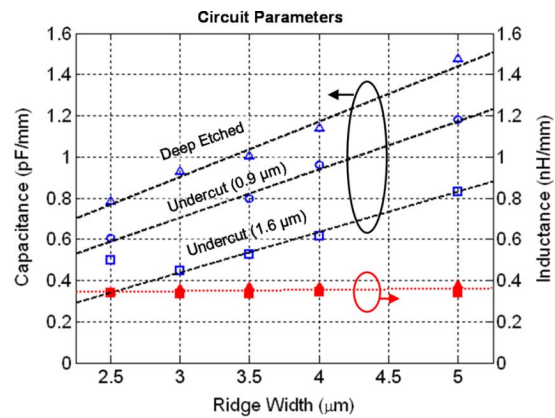


Fig. 5. TW-EAM capacitance and inductance per length.

exhibiting higher characteristic impedances. The EAMs with the most undercut exhibited the greatest increase in impedance with the exception of the $2.5\text{-}\mu\text{m}$ -wide ridge. In this device, the selective wet etch reduced the active region width to less than $0.9\ \mu\text{m}$ which was not structurally sufficient to support the upper cladding during the rest of the fabrication process. This device also suffered from high series resistance and high optical loss which confirmed that the ridge structure was damaged.

For InGaAsP-InP-based modulators, the optical group index is approximately 4, whereas the electrical index is typically much higher due to the slow-wave propagation which arises from the diode capacitance, resulting in a velocity mismatch limitation [7]. The measured electrical effective index for the same set of EAMs is shown in Fig. 4. The results show that the reduced capacitance of the narrowed ridge and undercut waveguide significantly lowers the electrical index. In the case of the $3.0\text{-}\mu\text{m}$ ridge, the index is reduced from 5.5 to 3.7 after the undercut etch, demonstrating that the electrical velocity can be designed to exceed the optical velocity.

From the impedance and index measurements, we have also extracted the capacitance and inductance per length of each of the structures (Fig. 5). As expected, the inductance is nearly constant for all of the devices since the metal electrodes are identical but the capacitance becomes significantly lower as the core width is reduced. The minimum capacitance achieved in these devices was $0.45\ \text{pF/mm}$ corresponding to a InGaAsP width of $1.4\ \mu\text{m}$.

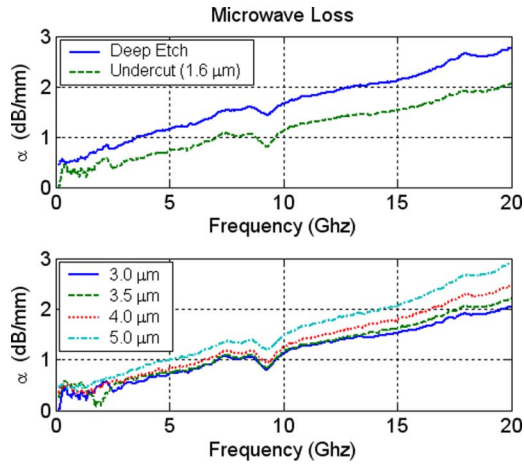


Fig. 6. Microwave loss parameter (α) (upper) comparing deep etched and undercut ($1.6 \mu\text{m}$) waveguides with for ridge width of $3.0 \mu\text{m}$ and (lower) comparing ridge width for undercut ($1.6 \mu\text{m}$) waveguides.

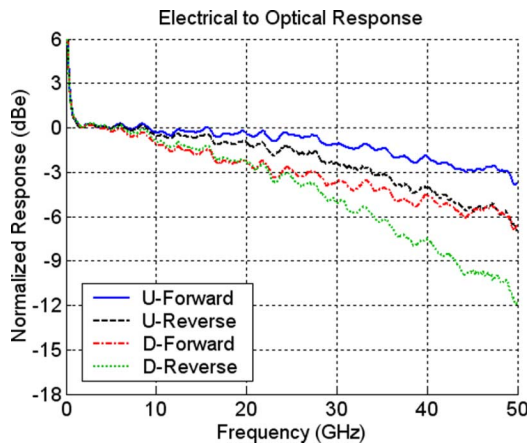


Fig. 7. Small signal E-O response for $3.0\text{-}\mu\text{m}$ deeply etched (D) and undercut (U) ($1.6 \mu\text{m}$) EAMs. “Forward” denotes copropagation and “Reverse” denotes counterpropagation of electrical and optical waves.

The TW-EAM structure is inherently lossy due to the diode resistance in series with the junction capacitance. However, extraction of the resistance values requires knowing the ratio of internal to external capacitance within the device [8]. Here, we have instead extracted the total microwave loss for both deep etched and undercut EAMs with $3.0\text{-}\mu\text{m}$ cladding and also for the undercut EAMs of varying ridge width (Fig. 6). In both cases, the loss decreases as the active region width is reduced. It is especially worth noting the reduced loss with decreasing ridge width, even though in this case the series diode resistance is higher. This is because α is proportional to $C^{3/2}$ but only linearly proportional to R and is, therefore, dominated by the junction capacitance [3].

IV. ELECTRICAL-TO-OPTICAL (E-O) RESPONSE

To demonstrate that the undercut waveguide is beneficial to the EAM performance, the E-O responses have been compared.

The response was measured on devices with a $26\text{-}\Omega$ integrated termination to be closely matched to the EAM impedance. The measurement was performed with an Agilent 8364A 50-GHz network analyzer and high-speed photodetector with a known frequency response. Light from an external laser source at $1.55 \mu\text{m}$ was coupled through the devices both forward and backward to compare the traveling-wave enhanced response. Fig. 7 shows the result of the E-O measurements for the $3.0\text{-}\mu\text{m}$ -wide modulators at -2.0-V reverse bias. In both devices, the increased response below 1 GHz is caused by the low-frequency limit of the on-chip capacitor. The undercut device 3-dB bandwidth is approximately 45 GHz compared with 25 GHz for the deeply etched device. Furthermore, the undercut modulator shows a 10-GHz enhancement in the forward traveling response compared with the reverse measurement, demonstrating the significance of the traveling-wave design.

V. CONCLUSION

We have presented an analysis of the microwave properties of TW-EAMs with selectively undercut active regions. We have shown that reducing the width of the waveguide core raises the characteristic impedance of the electrode by up to 35% and significantly lowers the microwave loss. Furthermore, the selective undercut can be used to reduce the junction capacitance sufficiently to achieve true velocity matching of the electrical and optical traveling waves. Using this fabrication technique, we have increased the 3-dB bandwidth of a $400\text{-}\mu\text{m}$ -long device from 25 to 45 GHz. These improved modulator designs can be incorporated with tunable lasers in future work on high-speed transmitters and monolithic wavelength converters.

REFERENCES

- [1] Y.-J. Chiu, T.-H. Wu, W.-C. Cheng, F. Lin, and J. Bowers, “Enhanced performance in traveling-wave electroabsorption modulators based on undercut-etching the active-region,” *IEEE Photon. Technol. Lett.*, vol. 17, no. 10, pp. 2065–2067, Oct. 2005.
- [2] H. Fukano, T. Yamanaka, M. Tamura, Y. Kondo, and T. Saitoh, “Very low driving-voltage InGaAlAs/InAlAs electroabsorption modulators operating at 40 Gbit/s,” *Electron. Lett.*, vol. 41, no. 4, pp. 211–212, Feb. 2005.
- [3] F.-Z. Lin, Y.-J. Chiu, and T.-H. Wu, “Cladding layer impedance reduction to improve microwave propagation properties in p-i-n waveguides,” *IEEE Photon. Technol. Lett.*, vol. 19, no. 5, pp. 276–278, Mar. 1, 2007.
- [4] M. Dummer, M. Sysak, J. Raring, A. Tauke-Pedretti, and L. Coldren, “Integration of a traveling-wave electro-absorption modulator with a widely tunable SG-DBR laser,” in *2007 Int. Conf. Indium Phosphide Related Mater.*, Matsue, May 2007, pp. 602–605.
- [5] S. Imscher, S. Imscher, R. Lewen, and U. Eriksson, “InP–InGaAsP high-speed traveling-wave electroabsorption modulators with integrated termination resistors,” *IEEE Photon. Technol. Lett.*, vol. 14, no. 7, pp. 923–925, Jul. 2002.
- [6] R. Spickermann and N. Dagli, “Experimental analysis of millimeter wave coplanar waveguide slow wave structures on GaAs,” *IEEE Trans. Microw. Theory Tech.*, vol. 42, no. 10, pp. 1918–1924, Oct. 1994.
- [7] R. Walker, “High-speed III–V semiconductor intensity modulators,” *IEEE J. Quantum Electron.*, vol. 27, no. 3, pp. 654–667, Mar. 1991.
- [8] R. Lewen, S. Imscher, and U. Eriksson, “Microwave CAD circuit modeling of a traveling-wave electroabsorption modulator,” *IEEE Trans. Microw. Theory Tech.*, vol. 51, no. 4, pp. 1117–1128, Apr. 2003.